Supplementary Material

Varied domain structures in $0.7Pb(Mg_{1/3}Nb_{2/3})O_3$-$0.3PbTiO_3$ single crystals

Dawei Zhang[1,2,#], Lei Wang[1,#], Linglong Li[3], Pankaj Sharma[4,5], Jan Seidel[1,2]

[1]School of Materials Science and Engineering, UNSW Sydney, Sydney, NSW 2052, Australia.

[2]ARC Centre of Excellence in Future Low-Energy Electronics Technologies, UNSW Sydney, Sydney, NSW 2052, Australia.

[3]Key Laboratory of Quantum Materials and Devices of Ministry of Education, School of Physics, Southeast University, Nanjing 211189, Jiangsu, China.

[4]College of Science and Engineering, Flinders University, Bedford Park, Adelaide, SA 5042, Australia.

[5]Flinders Institute for Nanoscale Science and Technology, Flinders University, Adelaide, SA 5042, Australia.

[#]Authors contributed equally.

Correspondence to: Prof. Jan Seidel, School of Materials Science and Engineering, UNSW Sydney, Sydney, NSW 2052, Australia. E-mail: jan.seidel@unsw.edu.au

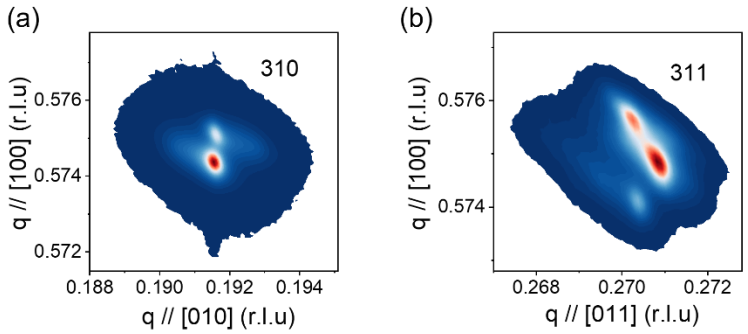

Figure S1. (a) and (b) RSM maps around 310 and 311 reflections of the single crystal, respectively.

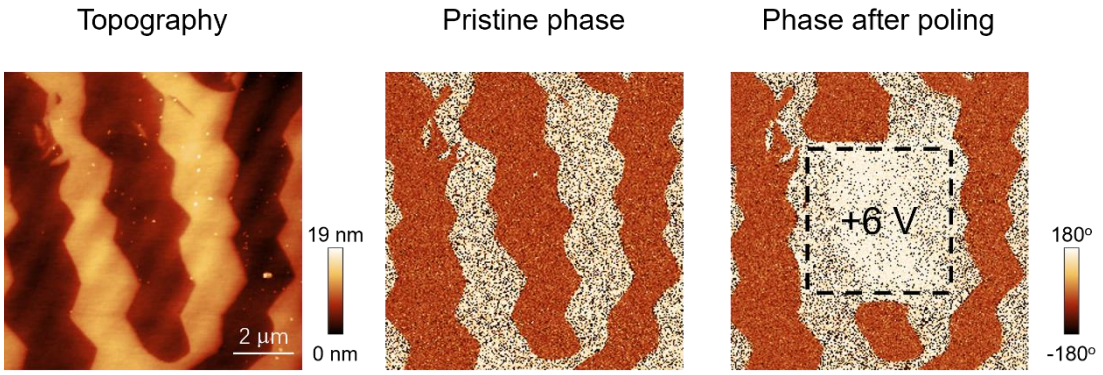

Figure S2. The OOP poling experiment with a tip bias of +6 V

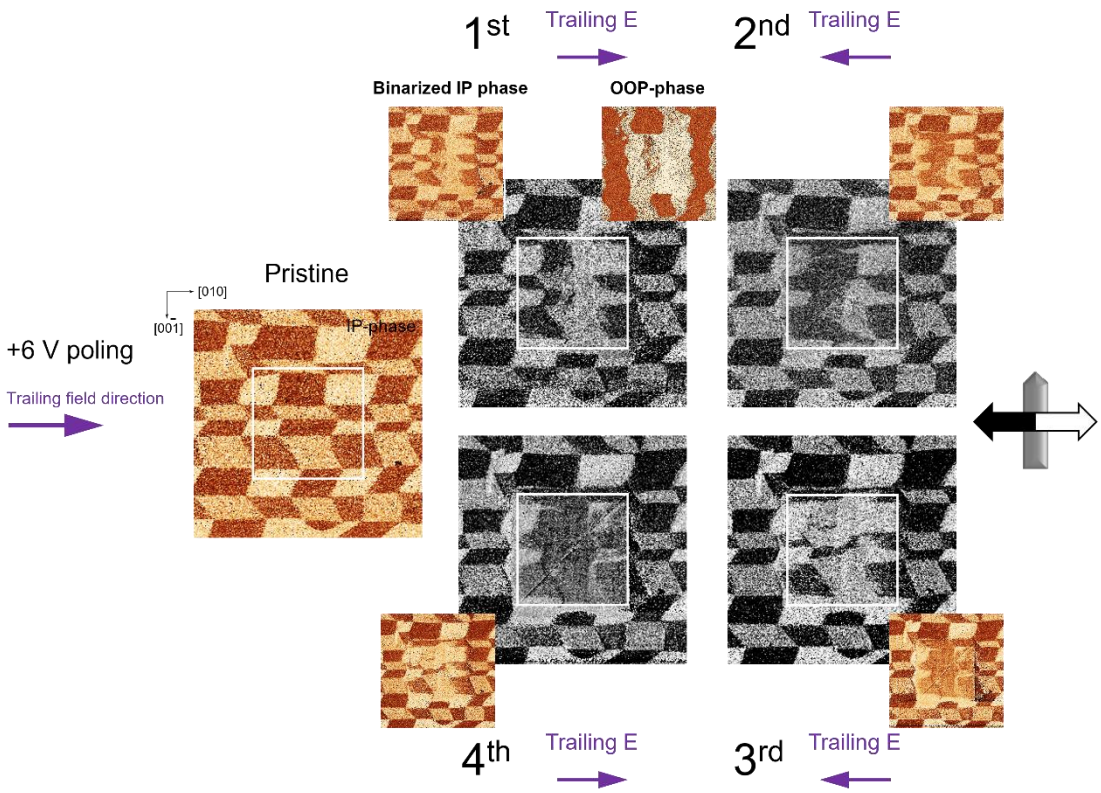

Figure S3. The trailing field experiment to determine the directions of the IP phase contrast. All the phase images shown here are IP phase signals unless otherwise denoted. All the measurements shown here were performed at off-resonance frequency. A tip bias of +6 V was used to pole the sample, and the trailing field direction was co-determined by the slow scan axis of the tip and the polarity of the tip bias, as denoted by the purple arrow. The trailing field experiments were performed four times in the denoted sequence. The original data was shown in the insets beside the binarized data. By comparing the directions of the trailing field and the resultant binarized contrast, the directions of the IP phase contrast can be determined.

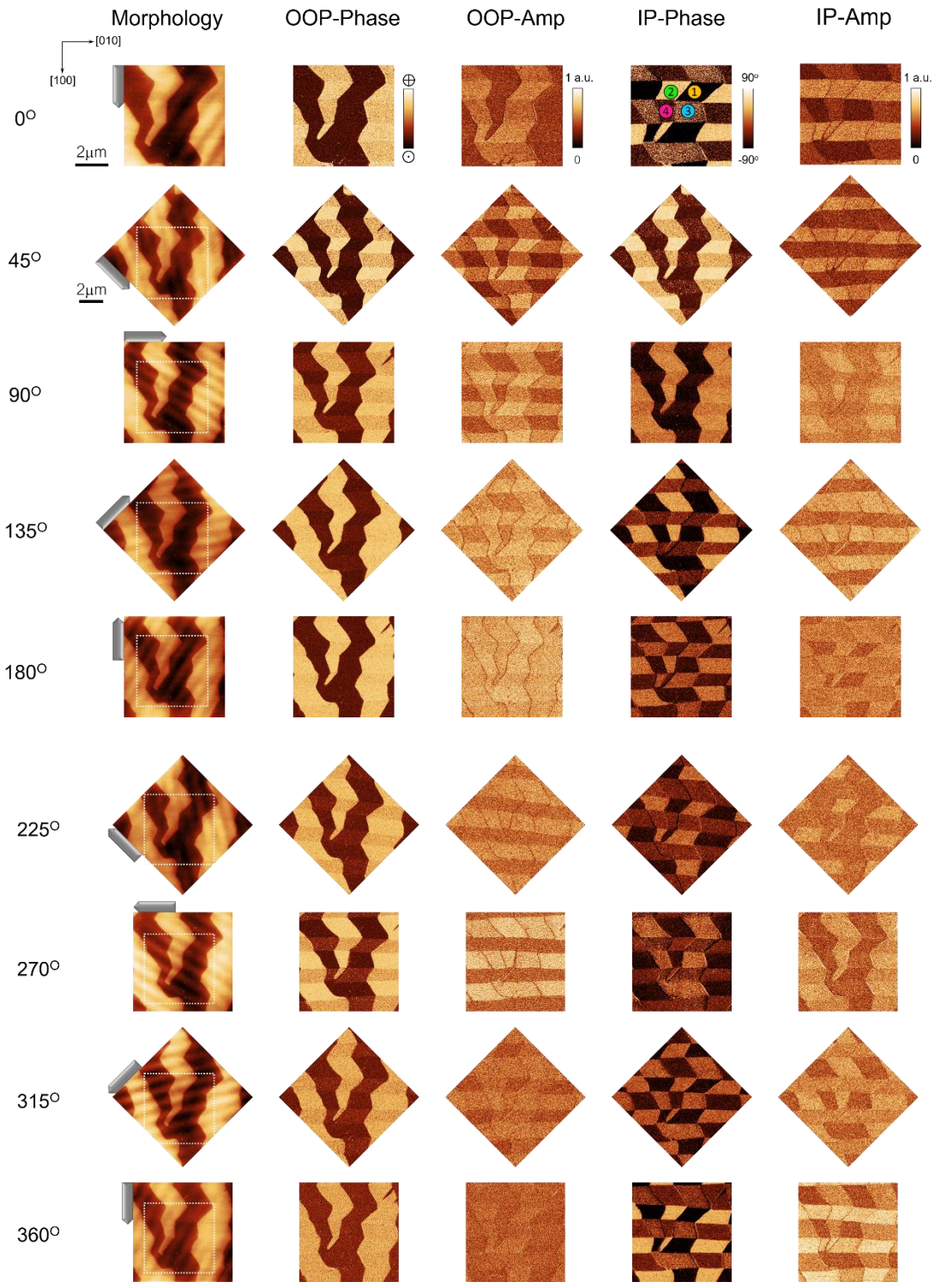

Figure S4. A full-range off-resonance angle-resolved PFM image with rotation angles from 0° to 360° with an interval of 45°. The image size for 0° is 6μm × 6μm and the image size for the rest of the rotation angles is 8μm × 8μm.

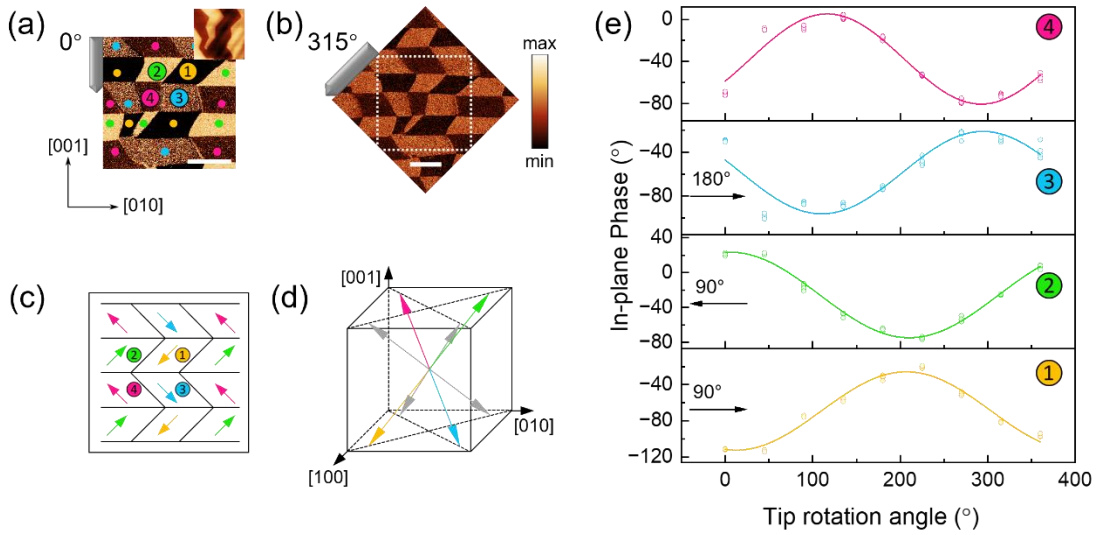

Figure S5. The domain and crystal structure of the PMN-PT single crystal. (a)-(b) Representative angle-resolved IP phase images of 0° and 315°. The white dashed boxes delineate the quasi-identical scanned area at 0°. The topography is also shown as an inset for the 0° IP phase. Cantilevers show sample rotation angles with respect to the $[00\bar{1}]$ direction. All the domains can be classified into four categories depending on their polarization variants (coloured dots). Both scale bars are 2 μm. (c) IP polarization directions for the four types of domains. (d) Three-dimensional model for polarization vectors in the PMN-PT single crystal. (e) Angle-dependent in-plane signals of four different domains are fitted to a trigonometric curve.

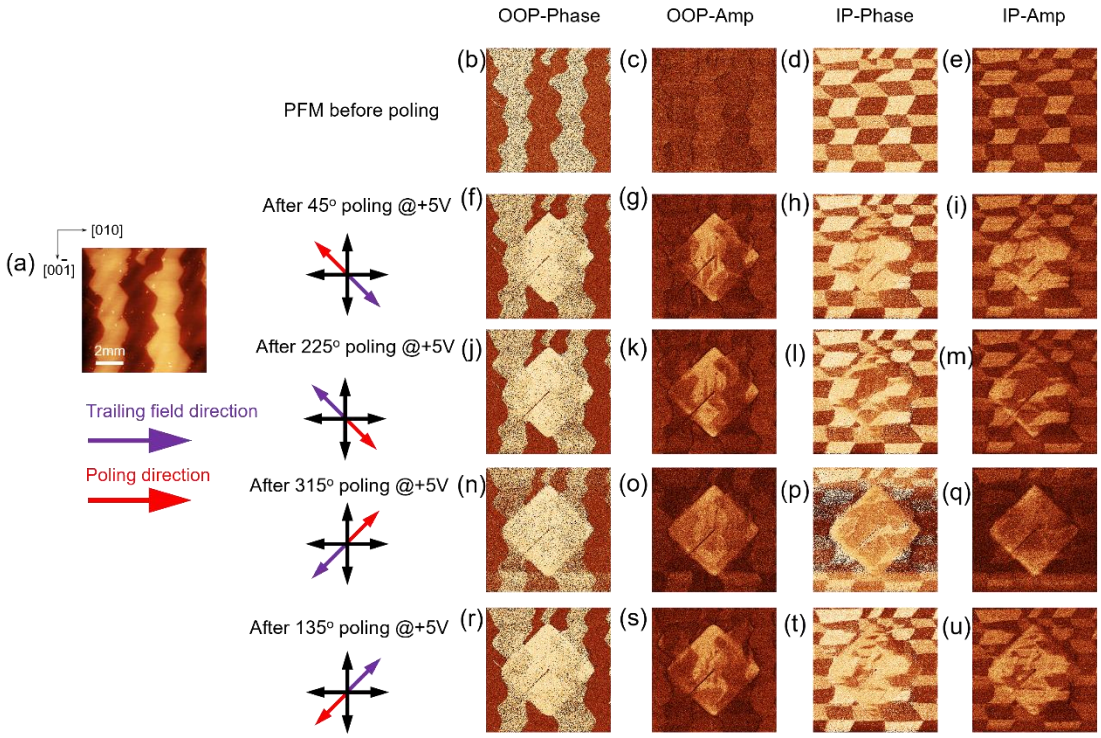

Figure S6. Trailing field experiments at +5 V with different angles. (a) The topography of the scanned area. (b)-(e) PFM images for the pristine state before DC poling. (f)-(i) PFM images after +5V poling with a 45° rotation angle. (j)-(m) PFM images after +5V poling with a 225° rotation angle. (n)-(q) PFM images after +5V poling with a 315° rotation angle. (r)-(u) PFM images after +5V poling with a 135° rotation angle. The purple and red arrows indicate the directions of the trailing field and poling field, respectively.

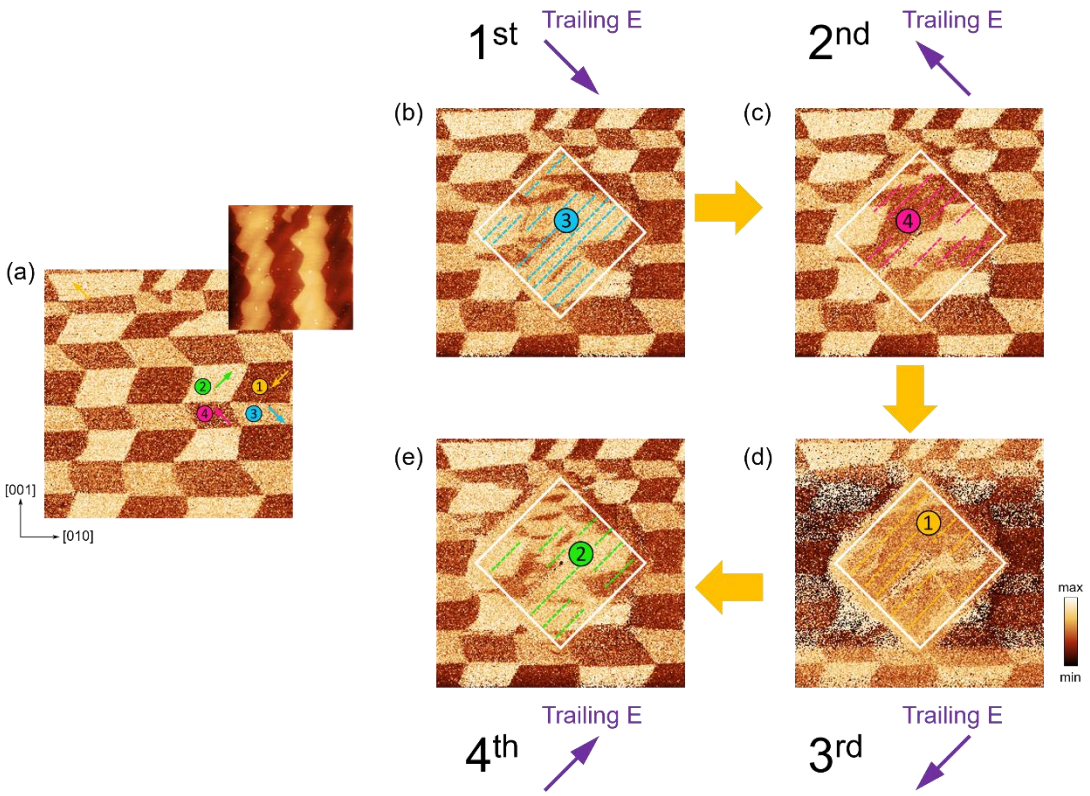

Figure S7. The analysis of the trailing field experiments. (a) The IP-phase image of the pristine state with the direction of four polarization variants is indicated by the colour arrows. (b)-(e) Trailing field experiments at +5 V with different rotation angles in sequence. The purple arrows in (b)-(e) show the directions of the trailing fields. The respective colours and dashed lines inside the poling area (delineated by the white dashed boxes) denote the IP polarization favoured by the direction of the trailing fields.

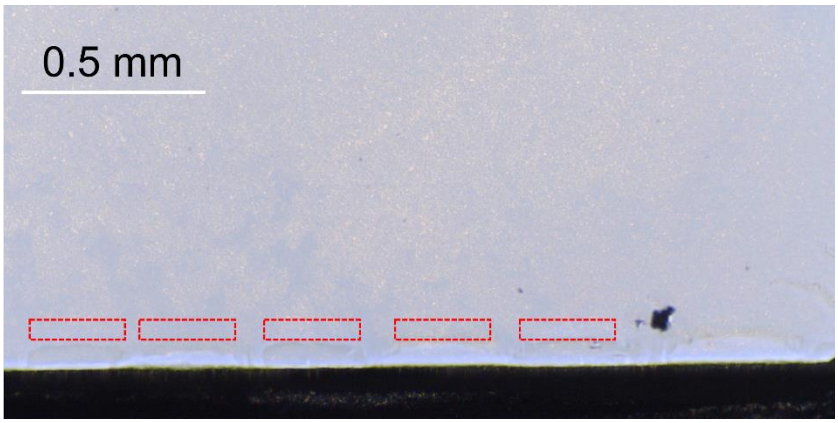

Figure S8. The optical image of the regions of the type 3 domain.

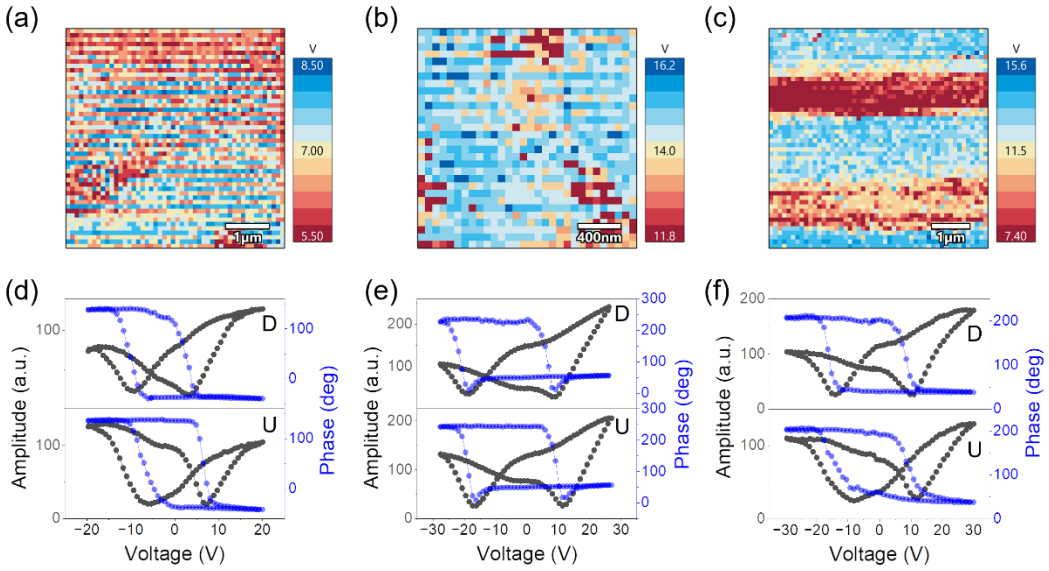

Figure S9. SSPFM mapping and corresponding averaged SSPFM curves. (a)-(c) SSPFM mapping for type 1, 2, and 3 domains, respectively. (d)-(f) The averaged SSPFM curves over 100 data sets each for upward and downward domains in type 1, 2, and 3 domains, respectively. 'D' and 'U' denote the downward and upward domains.

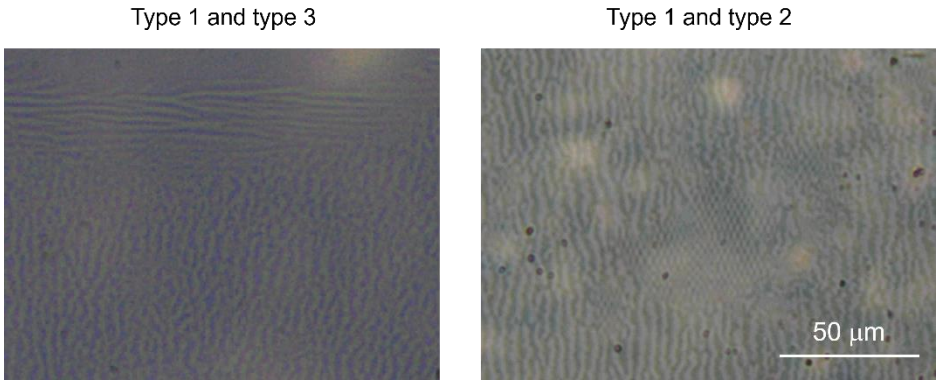

Figure S10. Optical microscope images (a) and (b) to show the cross-boundary regions between type 1 and type 3 domains, and between type 1 and type 2 domains, respectively.